# Diffusion of linear macromolecules and spherical particles in semidilute polymer solutions and polymer networks

Sebastian Seiffert, Wilhelm Oppermann*

Institute of Physical Chemistry, Clausthal University of Technology, Arnold-Sommerfeld-Strasse 4, D-38678 Clausthal-Zellerfeld, Germany

## ARTICLE INFO

## ABSTRACT

The dynamics of fluorescently labeled linear macromolecules and spherical particles that are enclosed in semidilute polymer matrixes was studied by fluorescence recovery after photobleaching. The experiments were designed such that the transition from a semidilute solution to a permanent network could be covered. This was achieved by employing a matrix polymer, polyacrylamide, carrying pendant dimethylmaleimide groups. Stepwise irradiation of such samples in the presence of a triplet sensitizer causes successive dimerization of the maleimides leading to progressive crosslinking.

Studies were performed with varying concentrations of matrix polymer (20–80 g L$^{-1}$) as well as different molar masses (200,000–1,300,000 g mol$^{-1}$) and particle radii (17 and 36 nm) of enclosed labeled probes. Results show notable differences between the behavior of linear and spherical tracers: while the mobility of flexible linear chains remains nearly unaffected by the transition from a semidilute polymer solution into a chemically crosslinked network, spherical tracers get completely immobilized when the degree of crosslinking exceeds a certain threshold.

## 1. Introduction

The comprehensive understanding of dynamic processes in semidilute or concentrated polymer solutions and in chemically crosslinked gels is a central problem in polymer science, having attracted a vast amount of experimental and theoretical work within the last decades [1–8]. Obtaining a consistent picture of the dynamic properties of such systems is of interest with respect to the gain of insight into fundamental mechanisms of polymer motion as well as to the derivation of structure–property relations. On the other hand, the diffusive behavior of active components that are enclosed in crosslinked or uncrosslinked polymer matrixes plays an important role in biophysics, separation techniques, and pharmaceutical applications.

For concentrated solutions or melts, the reptation model introduced by de Gennes [9–11] and Doi and Edwards [12–14] has led to significant progress. Basically, these scientists draw a picture of densely entangled polymer chains where the surrounding of a particular chain is modeled as a tube composed of long-living topological constraints that are imposed by neighboring chains. The tube confines the motion of the enclosed chain to creep along its own contour, while segmental displacements in directions perpendicular to the tube are largely restricted. The theoretical treatment of this situation leads to characteristic scaling relations for the dependence of the macroscopic translational diffusion coefficient $D$ on molecular weight $M$ and concentration $c$, namely

$$D \propto M^{-2} c^{(2-\nu)/(1-3\nu)} \tag{1}$$

where $\nu$ is the Flory exponent. In good solvents ($\nu = 0.6$), this corresponds to [10]

$$D \propto M^{-2} c^{-1.75} \tag{1a}$$

and in θ solvents ($\nu = 0.5$) to [15]

$$D \propto M^{-2} c^{-3} \tag{1b}$$

Later on, Schaefer et al. extended and revised the basic scaling and reptation theory by mean-field arguments for excluded volume interactions and derived the so-called marginal solvent model [16], which predicts

$$D \propto M^{-2} c^{-2.5} \tag{1c}$$

The assumption of fixed obstacles in the tube concept, meaning that the walls of the tube have to be long living on the time scale of chain motion, has been questioned. This approximation surely holds in entangled matrixes with chains that are markedly longer than a considered test chain or in the case of a crosslinked matrix, but may fail in the cases of weakly entangled systems. To account for fluctuations of the tube, a constraint release mechanism was suggested [17,18].

In semidilute polymer solutions of sufficiently low concentration, entanglements are not effective and the reptation model cannot be applied. Then, the polymers are considered to move like Rouse chains, and the scaling relation derived is:

$$D \propto M^{-1} c^{-(1-\nu)/(3\nu-1)} \tag{2}$$

In good solvents ($\nu = 0.6$), this leads to

$$D \propto M^{-1} c^{-0.5} \tag{2a}$$

whereas θ solvents ($\nu = 0.5$) show

$$D \propto M^{-1} c^{-1} \tag{2b}$$

The fact that one has to distinguish several concentration regimes where the mode of polymer motion is different and where different scaling predictions apply poses a problem when these predictions are to be experimentally verified, because the transitions between regimes are not precisely defined.

A fundamentally different approach to describe dynamic processes in polymer systems was introduced by Phillies, who suggested a universal scaling equation to describe the diffusion of various types of probes such as globular particles, linear chains, or star-shaped polymers in macromolecular matrixes over the entire concentration range from dilute to concentrated solution [19–26]:

$$D = D_0 \cdot \exp\left(-\alpha c^{\nu} M^{\gamma} R^{\delta}\right) \tag{3}$$

Herein, $D_0$ is the diffusion coefficient of the probe in dilute solution (assuming that there is no change of size or shape upon diluting), $R$ represents the probe radius, and $M$ and $c$ are the molecular weight and the concentration of matrix polymer. $\nu$, $\gamma$, and $\delta$ are scaling exponents, with $\nu$ being predicted to lie between 0.5 and 1. $\alpha$ has been theoretically treated in Ref. [22]. For polymer self-diffusion, Eq. (3) simplifies to

$$D = D_0 \cdot \exp(-\alpha c^{\nu}) \tag{3a}$$

with $D_0$ as the diffusion coefficient of an isolated macromolecule.

The latter relations were introduced empirically and it was shown that they describe a large amount of experimental data. Subsequently, Phillies presented a theoretical derivation of this so-called hydrodynamic scaling model, which is based on the assumption that hydrodynamic interactions significantly outweigh the effects of topological constraints [20–22]. An important feature of this approach is that there should be no fundamental differences between the diffusive behavior of flexible chains and rigid tracer particles.

Despite numerous experimental studies, a clear distinction against or in favor of one of the models of polymer motion has not been achieved. The scaling laws of reptation have been supported by early Forced Rayleigh Scattering (FRS) and dynamic light scattering (DLS) measurements performed by Leger et al. on polystyrene in good solvents [27–29]. Amis et al. studied polystyrene in good and θ solvents by DLS and found agreement with scaling predictions [30,31]. However, in a later paper they noted that it was necessary to take the effect of non-constant local friction into account to achieve agreement [32]. Other investigations on similar or other systems using pulsed field gradient NMR [33–36], FRS [37–39], FRAP [40], DLS [35,36,41], and single molecule tracking [42] also supported some of the scaling predictions, when semidilute solutions were considered in a limited concentration range. Much support for Phillies' equation stems from investigations dealing with the mobility of rigid, spherical particles suspended in polymer solutions [43–50]. The concentration dependence of the diffusion coefficient was in these cases well described by a stretched exponential function. Similar findings were reported for various biopolymer systems [51–56]. Comparison of the mobility of linear chains with that of well-defined star-shaped polymers in a polymer matrix, as in particular extensively studied by Lodge et al. [57–60], led to challenging the relevance of reptation, but demonstrated that Phillies' equation described the concentration dependence extremely well in a wide range from very dilute to semidilute solutions. Such comparisons were also discussed by Phillies himself [61,62] to support the hydrodynamic scaling model. In some instances, measured data were in agreement with *both* kinds of descriptions within experimental uncertainty [63–65]. However, experimental conditions frequently restricted the accessible concentration range or molecular weight range to within narrow bounds, so that it was difficult to reach a general conclusion.

In the present work, we study the diffusion of tracers in polymer matrixes while the matrix is being crosslinked. By investigating the influence of the sol–gel transition and of the rising crosslink density on tracer mobility, an additional new aspect is introduced that may be looked upon in view of different theoretical models. Although there are quite a few papers in the literature that consider the mobility of tracers enclosed in networks [49,52,55,66–76], a study of the *same* system in the sol *and* gel state and, especially, *during the sol–gel transition* has not been performed before.

We make use of a highly selective [2 + 2] photoaddition reaction to achieve progressive crosslinking of suitably functionalized polymer chains. That way we can start from a semidilute solution which contains the tracer molecules or tracer particles. After measuring the diffusion coefficient of the tracers in solution, the system is irradiated to attain a certain conversion of the crosslinking reaction. The conversion is then determined by UV spectroscopy, and subsequently another measurement of the diffusion coefficient is performed. This sequence of irradiation, characterization, and measurement steps is repeated until complete conversion of the photoreaction is achieved.

The diffusion coefficient is measured by fluorescence recovery after photobleaching (FRAP) of suitably labeled tracers. These are on the one hand linear macromolecules which carry few dye labels. By keeping the degree of labeling small (0.1 mol-%), we ensure that tracer molecules and matrix molecules are essentially identical. On the other hand, dye-labeled polystyrene nanospheres are employed. Parameters varied besides the gradual increase of the degree of crosslinking are the concentration of matrix polymer and the molecular weights or hydrodynamic radii, respectively, of the linear or spherical tracers. Fig. 1 schematically illustrates the intention of this approach.
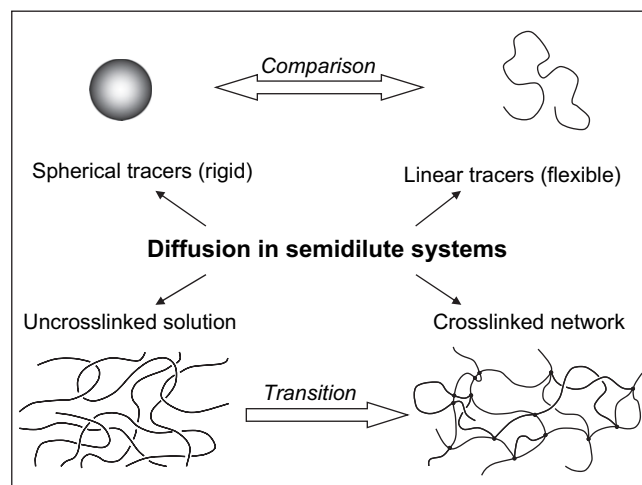


**Fig. 1.** Schematic illustrating the basic intention of the present work.

## 2. Consideration of the system studied

In this section, the chemical structures of the compounds employed are presented, and some general aspects of the reaction conditions and experimental parameters are discussed.

The polymers used are slightly modified poly(acrylamides) (PAAms) prepared by radical copolymerization, as described in detail in Section 3. The matrix polymer is a PAAm copolymer containing about 1.5 mol-% repeat units carrying dimethylmaleimide (DMMI) groups. Thioxanthone disulfonate (TXS) is employed as a triplet sensitizer. Then, irradiation of an aqueous solution with light of wavelength 382 nm (absorption maximum of TXS) induces dimerization of the DMMI moieties and thus leads to crosslinking of the correspondingly functionalized PAAm chains, as depicted in Fig. 2. A detailed investigation of the crosslinking reaction has shown that the DMMI dimers formed are in fact a mixture of two structures [77], both of which constitute a covalent link between two macromolecules. However, the photocrosslinking reaction proceeds in a highly efficient and well-controlled manner without perceptible side reactions. Its progress can be followed by UV spectroscopy. Making use of a sensitized reaction offers the great advantage that the concentration of crosslinkable polymer, which decisively controls the hydrogel structure eventually formed, can be adjusted independently of sensitizer concentration. The latter has to be chosen according to the absorption properties to avoid the build-up of a gradient over sample thickness.

To enable FRAP measurements for the determination of diffusion coefficients, the tracers were labeled with rhodamine B (or a corresponding dye for the spheres). Rhodamine B is readily bleached by irradiation with the 488 and 514 nm lines of an Ar laser, while this laser light does not affect the TXS or the DMMI moieties. On the other hand, UV light of wavelength $(383 \pm 6)$ nm, as used for inducing gelation, does not affect the dye labels since their absorbance in this wavelength range is negligible. The two photochemical processes, i.e., light-induced crosslinking of the matrix polymer and bleaching of the chromophore in a FRAP experiment, thus occur independently and do not interfere with each other. This
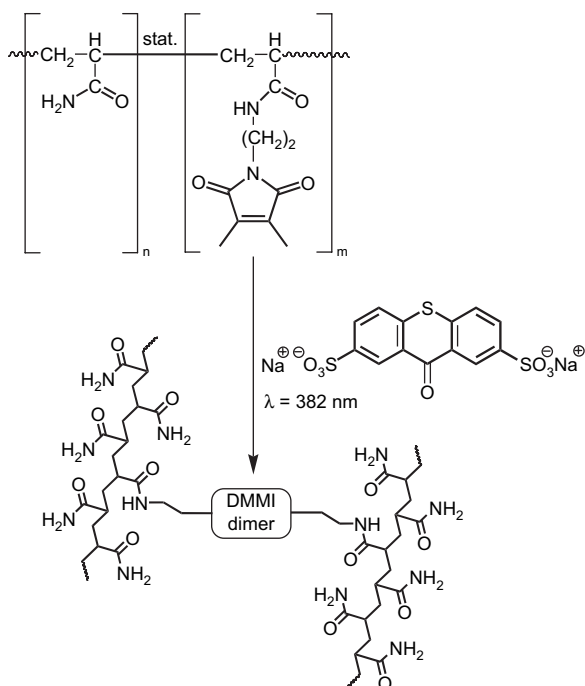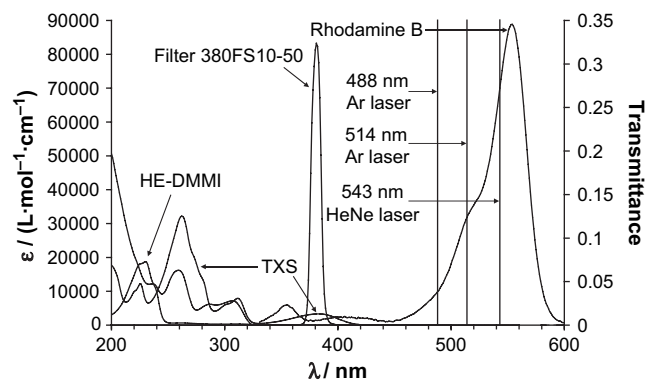
**Fig. 3.** Spectroscopic specification of the system studied. Left axis: UV–vis absorption coefficients of rhodamine B, thioxanthone disulfonate (TXS), and the DMMI chromophore as measured for the model compound N-(2-hydroxyethyl)-dimethylmaleimide (HE-DMMI) [77] in aqueous solution, respectively. Right axis: transmittance of the interference filter "380FS10-50" used to achieve TXS-sensitized photochemical DMMI dimerization. Also included are the laser lines employed for FRAP measurements.

important requirement is substantiated in Fig. 3, where the absorption spectra are shown of all chromophores present in the system, together with the laser lines and wavelength ranges used to irradiate the sample. Some photophysical data that are relevant for the present work are also compiled in Table 1.

The tracers employed were linear rhodamine B labeled polyacrylamides with different molar masses, prepared and characterized as described earlier (cf. Fig. 4) [78]. By using labeled PAAm tracers in a PAAm matrix, the difference in chemical structure could be minimized in order to exclude perturbations due to possible thermodynamic incompatibility. Commercially available red-labeled polystyrene microspheres having particle radii similar to the dilute-state hydrodynamic radii of the linear tracers were used for comparison.

The FRAP measurements were performed on a confocal laser scanning microscope (CLSM) and evaluated according to a procedure developed recently [79,80]. The recovery of fluorescence intensity is measured with high temporal and spatial resolution. This allows for the appropriate treatment of diffusion processes characterized by a distribution of diffusion coefficients, and the proper determination of mean values. Since the linear tracers exhibit some polydispersity, application of this method is essential to obtain reliable data.

By employing this FRAP approach, the diffusion coefficients are measured on a length scale of around 10 μm. The commonly observed inhomogeneities in networks or gels, which are responsible for the non-ergodicity detected, e.g., by light scattering, occur on a typical length scale of 5–50 nm [89–93]. The FRAP method thus averages over such spatial inhomogeneities. Also note that inhomogeneities are less pronounced when the networks are generated by subsequent crosslinking of macromolecules in semi-dilute solution, as performed in the present work, rather than by crosslinking copolymerization [94].

## 3. Experimental

### 3.1. Materials

#### 3.1.1. Poly(AAm-co-DMMIAAm) (matrix material)

Polyacrylamide randomly functionalized with dimethylmaleimide moieties was synthesized as described in detail in Ref. [77]. This material can be crosslinked via photo-induced dimerization of the DMMI moieties (cf. below). In the present study, a sample containing 1.53 mol-% of functionalized monomer units was

**Fig. 2.** Photocrosslinking of P(AAm-co-DMMIAAm) ($n/m \approx 65$) upon irradiation with UV light. Thioxanthone disulfonate acts as triplet sensitizer. Adapted from Ref. [77].

**Table 1**
Photophysical properties of the chromophores used in this work

| Property | Rhodamine B | | Thioxanthone disulfonate (TXS) | | Dimethylmaleimide (DMMI) | |
|---|---|---|---|---|---|---|
| | Value | Reference, remark | Value | Reference, remark | Value | Reference, remark |
| $\lambda_{max}$ (fluo. ex.)/nm | 558 | [78] | 381 | [81] | 229 | $\lambda_{max}$ from UV spectrum of the model compound HE-DMMI [77] |
| $\lambda_{max}$ (fluo. em.)/nm | 583 | [78] | 437 | [81] | – | No detectable fluorescence |
| $E_S$/kJ mol$^{-1}$ | 210 | Derived from 0–0 transition in fluorescence spectra | 293 | Derived from 0–0 transition in fluorescence spectra | $\sim 520$ | Simply approximated from $\lambda_{max}$ in UV spectrum |
| $E_T$/kJ mol$^{-1}$ | 180 | Non-aqueous but polar medium [82] | 274 | Thioxanthone in nonpolar media [83] | 255 | Value for related dimethylmaleic anhydride [85] |
| | | | 267 | Thioxanthone in acetonitrile [84] | | |
| $\tau_S$/ns | 1.6 | [78] | 6.8 | [81] | – | |
| $\tau_T$/μs | 250 | Non-aqueous but polar medium [82] | 109 | [81] | – | |
| $\phi_{isc}$ | 0.005 | Non-aqueous but polar medium [82] | $\sim 1$ | Value for thioxanthone [86]; may appear reduced in polar media [84, 87] | 0.03 | Value for parent maleimide [88] |

$\lambda_{max}$ (fluo. ex.): wavelength for maximum fluorescence excitation, $\lambda_{max}$ (fluo. em.): wavelength of maximum fluorescence emission, $E_S$: energy level of the first excited singlet state, $E_T$: energy level of the first excited triplet state, $\tau_S$: average lifetime of the first excited singlet state, $\tau_T$: average lifetime of the first excited triplet state, $\phi_{isc}$: quantum yield of intersystem crossing. If not otherwise stated, values are reported for aqueous media.

employed (denoted PAAm–DMMI2.0). Several characteristic data are listed in the first line of Table 2.

### 3.1.2. Fluorescently labeled polyacrylamide (linear tracers)

Rhodamine B labeled polyacrylamides used as linear tracers were prepared and characterized as described in Ref. [78]. Four different molar masses were available. The relevant properties of these materials are also compiled in Table 2. Further characteristics, in particular the spectroscopic properties, may be found in Ref. [78] and in Table 1.

The molar masses of the linear tracers were chosen such that the range from smaller to equivalent and larger than that of the matrix polymer was covered. Note, however, that the molar masses quoted in Table 2 were determined by SEC calibrated with pullulan standards (for details on SEC measurements cf. Refs. [77,78]). Hence, the absolute values might be somewhat different. The polydispersity of the samples is rather large and increases with rising chain length. Translational diffusion coefficients can be expected to exhibit a corresponding distribution. Although our recently published procedure for FRAP analysis is well suited to deal with such distributions and to determine reliable mean values [80], molar mass dependencies should be discussed with particular care.

### 3.1.3. Microspheres (spherical tracers)

Fluorescently labeled polystyrene microspheres with nominal diameters of 24 and 40 nm were purchased from Molecular Probes,

Eugene, OR, USA (red fluorescent carboxylate-modified Fluo-Spheres, 580/605, LOT: 24 nm: 44023A; 40 nm: 21774 W) as aqueous suspensions with concentrations of 2 and 5 wt.-% solids, respectively. They were extensively characterized by UV–vis spectroscopy, fluorescence spectroscopy, dynamic light scattering, ultracentrifugal analyses, atomic force microscopy, and FRAP.

The spectroscopic analyses revealed that the label employed provides characteristics similar to rhodamine B. The particle sizes obtained by various methods are compiled in Table 3. Both types of spheres are somewhat bigger than stated by the manufacturer. For the spheres having the larger nominal diameter, there is an appreciable variation between the results obtained by different methods, whose origin could not be clarified. However, since the FRAP method was used to determine the diffusion coefficient in different environments, we will refer to the hydrodynamic radii determined by FRAP in dilute suspension (17 and 36 nm) to identify the microspheres.

### 3.2. Experimental techniques

#### 3.2.1. Spectral characterization of probes

*3.2.1.1. UV–vis spectroscopy.* All UV–vis spectra were measured on a Jasco V550-spectrometer in the range of 190–700 nm. For a basic characterization of the labeled species, test solutions of appropriate concentration were investigated in 1 cm quartz cuvettes (Hellma). Results obtained in this manner (cf. Table 1) were just needed for a proper adjustment of concentrations and irradiation conditions for the photo-induced crosslinking experiments. The determination of the conversion of photoreactive DMMI groups by UV spectroscopy was performed on sample cuvettes with layer thicknesses of 100 μm (Hellma) as described further below.

*3.2.1.2. Fluorescence spectroscopy.* Fluorescence spectra for characterization of the labeled species were recorded on a Spex Fluorolog II photon counting spectrometer employing the same solutions as used for UV–vis spectroscopy. Results were again solely needed for adequate adjustment of the irradiation conditions used for crosslinking (cf. Table 1 and Refs. [78,80] for details).

#### 3.2.2. Characterization of probe sizes and mobilities

*3.2.2.1. Ultracentrifugal analysis.* Ultracentrifugal analyses were performed on a commercial analytical ultracentrifuge of type OPTIMA XL-A 70 from Beckmann–Coulter detecting the UV–vis absorbance of the fluorescently labeled species. Estimations of the
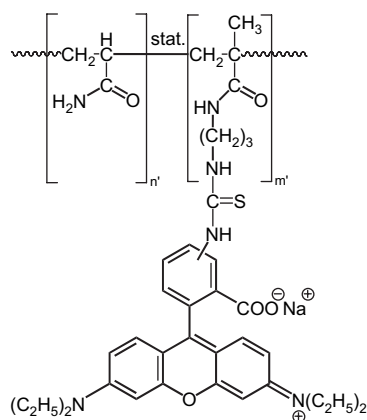


**Fig. 4.** Structure of rhodamine B labeled polyacrylamide as prepared in the context of Ref. [78]. Samples used in the present work were composed according to $n'/m' \approx 1000$ in each case.

**Table 2**
Properties of the functionalized polyacrylamides employed for the present work

| Name of sample | Origin | Type | Functionalization | $M_N$[a] (g mol$^{-1}$) | $M_W$[a] (g mol$^{-1}$) | $M_W/M_N$ | $r_H$ (nm) | $c^{*b}$ (g L$^{-1}$) | $c^{*c}$ (g L$^{-1}$) |
|---|---|---|---|---|---|---|---|---|---|
| PAAm–DMMI2.0 | [77] | Matrix | 1.53 mol-% DMMI | 241 500 | 574 500 | 2.4 | 21.4 ± 3.4[d] | 2.7 | 5.2 |
| PAAm–C0.1–2 | [78] | Tracer | 0.11 mol-% rhodamine B | 423 000 | 1 280 000 | 3.0 | 52.1 ± 1.7[e] | 0.4 | 4.0 |
| PAAm–C0.1–3 | [78] | Tracer | 0.09 mol-% rhodamine B | 232 000 | 590 000 | 2.5 | 25.3 ± 3.8[e] | 1.7 | 5.9 |
| PAAm–C0.1–4 | [78] | Tracer | 0.13 mol-% rhodamine B | 134 000 | 348 500 | 2.6 | 16.2 ± 0.6[e] | 3.8 | 8.6 |
| PAAm–C0.1–5 | [78] | Tracer | 0.09 mol-% rhodamine B | 88 350 | 201 000 | 2.3 | 11.9 ± 0.9[e] | 5.5 | 13.3 |

$M_N$: number average molecular weight, $M_W$: weight average molecular weight, $r_H$: hydrodynamic radius in dilute aqueous solution, $c^*$: overlap concentration.

[a] Obtained as pullulan equivalent values by size exclusion chromatography (cf. Refs. [77,78] for details).
[b] Calculated as $c^* = ((3M_W)/(4\pi R_G^3 N_A))$ with $R_G = 2.05\ r_H$ [89] the radius of gyration and $N_A$ the Avogadro number.
[c] Estimated by solution viscometry in 0.5 mol L$^{-1}$ aqueous NaCl at $T = 25$ °C, employing $c^* = 1/[\eta]$ with $[\eta]$ the intrinsic viscosity.
[d] Estimated by dynamic light scattering on fairly dilute solution well below $c^*$ ($T = 25$ °C).
[e] Estimated by FRAP on pure tracers at concentrations of 5 g L$^{-1}$ ($T = 25$ °C).

sedimentation coefficient, $S$, were conducted by several runs at three different rotational velocities (8000–12 000 rpm) at 25 °C. The hydrodynamic radii were calculated via $r_H = (9\eta_D S/2(\rho_P - \rho_D))^{1/2}$, where $\eta_D$ denotes the viscosity of the dispersing medium (0.89 mPa s), $\rho_D$ its density (0.997 g mL$^{-1}$), and $\rho_P$ the density of the polymer microspheres (1.054 g mL$^{-1}$).

*3.2.2.2. Dynamic light scattering.* Dynamic light scattering was measured at 25 °C on an ALV/CGS-3 compact goniometer system S/N: CGS3-A0-028 from ALV GmbH using a HeNe laser at $\lambda = 632.8$ nm for irradiation as well as an ALV/LSE 5003 correlator. After filtering and diluting the test solutions to appropriate concentrations, several measurements were performed at scattering angles of 60°, 90°, and 120° and intensity-weighted distributions of the hydrodynamic radii were deduced from the correlation curves by simple fitting procedures provided by the ALV software. For the polystyrene microspheres, the angular dependence was not significant, and results were averaged to determine the mean hydrodynamic radii.

*3.2.2.3. Atomic force microscopy.* To quantify the static (i.e., the non-hydrodynamic) particle diameters of the spherical probes, surface imaging via TappingMode Atomic Force Microscopy was performed with a Nanoscope III (Digital Instruments). Ultrasharp, non-contact silicon cantilevers (pointprobes, type NCH-W, nanosensors, Sunnyvale, CA, USA) with resonance frequencies varying between 260 and 330 kHz were applied. Cantilever and tip were cleaned by immersion in and rinsing with ethanol.

Prior to use, mica plates were freshly cleaved by applying sticky tape yielding clean surfaces. The microsphere samples were prepared by placing the appropriate mica plates for 5 min upright into a dilute microsphere suspension with a concentration of about 0.5 wt.-%. Placing them upright and not horizontal avoids potential artifacts due to settled aggregates and therefore, it is ensured that only diffusion contributes to the resulting adsorption process. Afterwards, samples were gently dipped into deionized water and finally vacuum-dried for 12 h. In the end, this procedure yielded isolated or merely slightly grouped spheres on the mica

**Table 3**
Radii of the microspheres employed for the present work as estimated by dynamic light scattering (DLS), ultracentrifugal analysis (UA), atomic force microscopy (AFM), and fluorescence recovery after photobleaching (FRAP)

| Method | $r$ (17 nm microspheres) (nm) | $r$ (36 nm microspheres) (nm) |
|---|---|---|
| DLS | 16.7 | 51.5 |
| UA | 14.0 | 21.0 |
| AFM | 12.2 ± 3.8 | 21.5 ± 2.5 |
| FRAP | 16.6 | 35.8 |

Margins of error given for the AFM data reflect the standard deviation of the particle size distribution observed by this technique (histograms of particle sizes obtained from AFM analyses are shown in Fig. 5c and d).
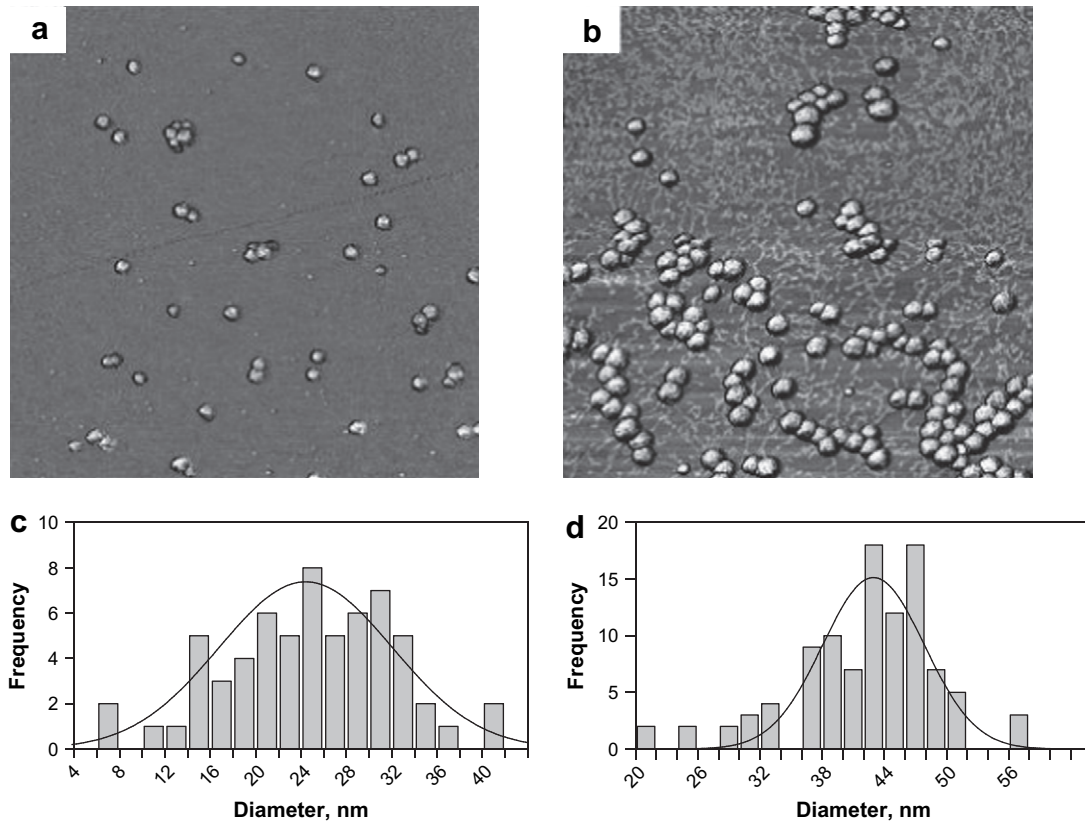
plates. AFM images obtained from these samples are presented in Fig. 5a and b.

Diameters of the microspheres were accessible by using the depth analysis command of the AFM software. As this provided merely reasonable results for isolated spheres, denser adsorbed areas were further investigated by determination of the height distance between peak and valley through the section analysis procedure. Histograms of particle diameters obtained from AFM images as the ones in Fig. 5a and b are shown in Fig. 5c and d.

*3.2.2.4. FRAP.* FRAP experiments were performed on a Leica TCS SP2 confocal laser scanning microscope using a 10× DRY objective of NA = 0.3. When the scanning mode was applied, the fluorophores were excited with the 543 nm line of a HeNe laser at 50% of its maximum power (0.22 mW at the object level). Bleaching was accomplished by irradiation of the fluorophores with the 543 nm line of the HeNe laser and the 514 and 488 nm lines of an Ar laser, each with full power (i.e., 0.22, 7.0, and 6.2 mW at the object level, respectively). Further settings were: Beam expander = 3, resolution = 256 × 256 pixels, zoom = 20 (which led to an image size of about 80 × 80 μm), and line scanning speed = 1000 Hz in the bidirectional scanning mode, when analyzing fast diffusion processes (e.g., when characterizing the pure tracers in the absence of polymer matrix). By contrast, slower processes as being observable within polymer matrixes were analyzed with resolution = 512 × 512 pixels, zoom = 32 (which led to an image size of about 50 × 50 μm), and line scanning speed = 800 Hz in unidirectional manner.

All samples for FRAP experiments were placed in the same quartz cuvettes having a layer thickness of 100 μm, which were also used for UV–vis spectroscopy. The confocal plane was set to be approximately in the middle of the specimen. Note that with choosing the 10× objective having a comparatively low NA, bleaching does not create any appreciable gradient in the z-direction. Thus we only have to consider two-dimensional lateral diffusion.

Before bleaching, a stack of 10 images was scanned to record the prebleach situation. For bleaching a point into the confocal plane, a chosen spot was irradiated for 3 s with the laser settings mentioned above. After bleaching, a series of 20 images was recorded to document the recovery process in each experiment. The sampling rate was about 5 fps in the case of fast diffusion processes or about 0.1–1 fps in the case of slower diffusing probes. The $e^{-1/2}$-radius of the bleached spot observed in the first image was typically 1.5–7 μm depending on the system analyzed. All experiments were conducted at a temperature of $(25 \pm 0.1)$ °C.

Some selected radially averaged intensity profiles obtained in this work are shown in Fig. 6. The evaluation procedure is described in detail in Refs. [79,80]. In the following, we just give a brief outline.

**Fig. 5.** AFM images of fluorescent polystyrene microspheres and histograms of particle diameters. Panels (a) and (c) correspond to the particles termed "17 nm spheres", (b) and (d) to the "36 nm spheres". Image size in (a) and (b) is 1 μm × 1 μm.

The solution to Fick's second law for two-dimensional diffusion in an infinite medium, where the initial concentration profile at $t = 0$ is a line sink (negative delta function due to bleaching), is given by

$$C(r,t) = C_0 - \frac{M}{4\pi Dt} \cdot \exp\left(\frac{-r^2}{4Dt}\right) \qquad (4a)$$

Here, $C(r,t)$ is the concentration of the fluorescently labeled species, being proportional to the measured fluorescence intensity. $D$ is the translational diffusion coefficient, $r$ the radial distance from the center of the bleached spot, and $M$ represents the amount of bleached substance per length in $z$-direction. $C_0$ is the prebleach or background concentration. Concentration profiles at finite times are thus negative Gaussians having an $e^{-1/2}$-radius of $\sqrt{2Dt}$ that sit on a constant background.

In real experiments, bleaching takes a finite time and does not produce a delta pulse on the spatial scale. Hence the actual starting conditions are not as just described. However, the real situation can adequately be accounted for by introducing a time lag $t_0$, a procedure equivalent to starting from a Gaussian with small but finite width $w_0$ (Eq. (4b)). This approach holds shortly after cessation of the bleach pulse.

$$C(r,t) = C_0 - \frac{M}{4\pi D(t + t_0)}e^{\frac{-r^2}{4D(t+t_0)}} = C_0 - \frac{M}{4\pi Dt + 2\pi w_0^2}e^{\frac{-r^2}{4Dt+2w_0^2}}$$
$$(4b)$$

The data points of a whole set of images then can be fit to Eq. (4b) to evaluate $D$. Since we are recording the fluorescence recovery data as a function of time and with high spatial resolution, the performance of the fit clearly indicates whether the diffusion process studied is adequately described by one single diffusion coefficient or whether a distribution of diffusion coefficients exists. In the latter case, Eq. (4b) has to be replaced by Eq. (4c), where a superposition of the individual profiles of all diffusing (fluorescent) species $i$ is assumed:

$$C(r,t) = \sum_i C_i(r,t) = C_0 - \sum_i \frac{M_i}{4\pi D_i(t + t_{0,i})}e^{\frac{-r^2}{4D_i(t+t_{0,i})}} \qquad (4c)$$

The fitting procedure starts out from discrete $D$ values evenly spaced on a logarithmic scale (typically 10 per decade) and covering the whole range of interest. These values are kept fixed, whereas their weightings, $M_i$, are adjusted through a number of iteration cycles to obtain the best agreement between experimental and simulated concentration profiles in the whole time domain studied. $D$ values with weightings of zero or negative are omitted in subsequent cycles. Eventually, this yields a discrete distribution of diffusion coefficients (that is, pairs of $D_i$ and $M_i$) without any need for calibration measurements (other than that of the length scale of the microscope). Since there is some arbitrariness in the choice of the individual $D$ values, the final results will be represented as continuous curves.

Corresponding calculations were automatically performed by a MATLAB software developed for this purpose. The typical recovery profiles and fit curves shown in Fig. 6 demonstrate the absence of undesired effects such as parasitic bleaching during the scanning procedure. Initial bleach depths were about 60% in each case, and the ratio of the duration of scanning and the duration of bleaching was about 6–60, depending on the system investigated. As shown in Refs. [79,80], the evaluation procedure employed for the present work does not produce artifacts in cases with comparably strong bleach depths and, additionally, is able to deal with situations were the time required for bleaching is comparable to or even exceeds the typical time for fluorescence recovery. Other investigators
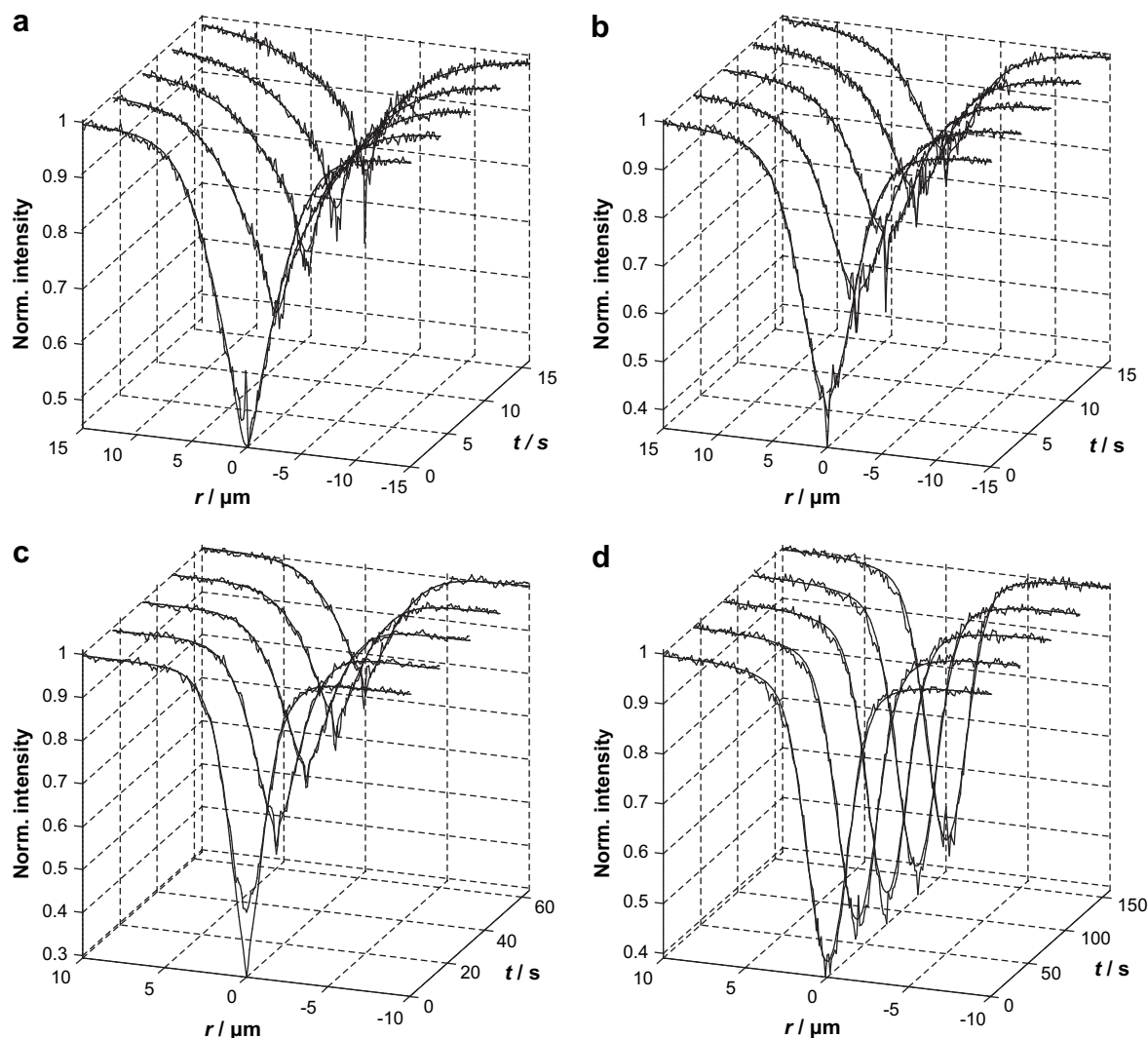
**Fig. 6.** Fluorescence recovery profiles (noisy lines) and fit curves according to Ref. [80] (smooth lines) as obtained for 60 g L$^{-1}$ PAAm–DMMI2.0 matrixes containing trace amounts of fluorescently labeled polyacrylamide PAAm–C0.1–4 (a and b) or 17 nm polystyrene nanospheres (c and d) prior to gelation (a and c) or well beyond the gel point (b and d). For greater clarity, *r*-axes are zoomed in and each figure solely depicts 5 out of 20 profiles.

demonstrated [53] that similar spatially resolved FRAP experiments were not affected to a measurable extent by parameters such as the size, position, and depth of the bleached spot.

### 3.3. Preparation of samples for systematic investigations

#### 3.3.1. Samples containing linear tracers

Samples for the experimental series described below were simply prepared by dissolution of appropriate amounts of matrix and tracer material as well as thioxanthone disulfonate (TXS) as a photosensitizer in water. Matrix concentrations were 20, 40, 60, and 80 g L$^{-1}$, which all lie above the overlap threshold $c^*$ (cf. Table 2). Fluorescently labeled linear tracers were included in amounts of 5 g L$^{-1}$. This concentration does or does not exceed the corresponding $c^*$ depending on whether one regards $c^{*b}$ or $c^{*c}$ from Table 2. Hence, it is not clear whether or not the labeled chains overlap with each other; however, they do certainly overlap with the matrix polymer.

Volumes prepared were 1 mL in each case. Homogenization of the semidilute solutions was achieved by allowing them to stand for several days. Finally, droplets of each solution were placed in quartz cuvettes with a layer thickness of 100 µm (Hellma). Note that the concentrations of DMMI moieties in the samples thus

prepared lay between 4 and 16 mmol L$^{-1}$. The concentration of TXS was 1 mmol L$^{-1}$ in each case.

#### 3.3.2. Samples containing spherical tracers

When microspheres were to be enclosed in photo-crosslinkable matrixes, this was achieved by dissolving 20–80 g L$^{-1}$ of the matrix polymer PAAm–DMMI2.0 directly in parent suspensions containing 0.5 wt.-% of spheres together with 1 mmol L$^{-1}$ of TXS and 0.01 mol L$^{-1}$ of NaOH. (The addition of base should ensure sufficient deprotonation of the spheres' surficial carboxylic groups. Some experiments involving linear tracers were carried out in acidic, neutral, and basic media. The results obtained were absolutely independent of pH. This proves that a consistent comparison between measurements on spherical and linear tracers is permitted, despite different pH values.) Volumes prepared were again 1 mL, respectively, and sample homogenization was achieved by equilibration over a period of several days. Samples were then placed in quartz cuvettes with a layer thickness of 100 µm.

### 3.4. Schedule for systematic investigations

Systematic investigations of tracer mobility as a function of progressive crosslinking were performed in the following manner:

we generally start from a semidilute solution composed of matrix and tracer that has been prepared as described in Section 3.3. After measuring the diffusion coefficient in a series of FRAP experiments in the manner described in Section 3.2, the sample was irradiated with UV light for some time in order to achieve a partial conversion of DMMI dimerization. The light source employed was a 6 W laboratory UV lamp of type NU-6K1 (Konrad Benda Laborgeräte u. Ultraviolettstrahler, Wiesloch, Germany) providing spatially homogeneous irradiation with a relatively broad spectrum in the range of $(365 \pm 20)$ nm. Further spectral selection was achieved by introducing a narrow-band interference filter of type 380FS10-50 (LOT Oriel, Darmstadt, Germany), which confines the irradiation range to be $(383 \pm 6)$ nm (cf. Fig. 3). Samples placed in 100 μm cuvettes were irradiated at a distance of 35 mm, corresponding to an intensity of about 15 μW cm$^{-2}$. At regular intervals, UV exposure was interrupted and samples were analyzed by UV–vis spectroscopy and FRAP to quantify the actual conversion of DMMI (degree of crosslinking) and the tracer mobility, respectively. This procedure was repeated until the sample was fully crosslinked. Every FRAP experiment was repeated five times at different, randomly chosen positions (on a mm scale) within one sample to check for reproducibility and spatial variance.

For practical handling, we always worked with sets of six samples of the same matrix concentration, each one of them containing one out of the four linear or two spherical tracers. All samples of one set were irradiated simultaneously and analyzed at the same intervals. The individual conversions of DMMI in each set were then averaged to obtain a mean value for each matrix concentration.

The photo-induced crosslinking of the matrix polymer has been studied in detail before [77]. The crosslinking reaction can be well controlled by adjusting the amount of sensitizer and the intensity of irradiation, the rate of DMMI conversion being proportional to either of these two quantities. Due to this simple dependency, it was possible to reduce the concentration of TXS down to a comparatively low value of 1 mmol L$^{-1}$, ensuring sufficient transmittance of UV light ($>$90%) through the sample layer (100 μm) and thus avoiding formation of a gradient in z-direction. Homogeneous gelation in x- and y-direction was realized by use of a UV lamp that provides spatially homogeneous irradiation.

The conversion of DMMI was determined by quantifying the change of UV absorbance at 229 nm as described in detail in Ref. [77]. The absorption band characteristic of DMMI moieties is superimposed on a background predominantly resulting from the PAAm backbone, but also from the TXS sensitizer and to a minor extent from the rhodamine labels of the tracers. These spectral contributions were subtracted before calculating the conversion.

When spherical tracers were employed, the strong UV absorbance of the polystyrene beads prevents this kind of analysis. Therefore, reference samples were prepared having the same composition but not containing microspheres. These were irradiated simultaneously with the actual samples. The UV analysis was then performed on the reference samples. The presence of the microspheres also led to an attenuation of the 383 nm light used to initiate the crosslinking reaction. This effect was taken into account by correcting the conversion data determined on the reference samples by a factor of 0.66, which is the ratio of sample transmittance in the range of $(383 \pm 6)$ nm with and without microspheres. Moreover, only data obtained at conversions below 0.6 were considered. In samples containing linear tracers, however, the concentration of rhodamine B labels was so small (0.07 mmol L$^{-1}$) that they did not cause any perceptible absorbance at around 383 nm, so that no correction was necessary.

From the data of DMMI conversion with time, the corresponding elastically effective network densities were calculated based on the report in Ref. [77]: effective network densities were obtained from modulus measurements, and it was shown that the rise of modulus with time occurs in proportion with DMMI dimerization. (The material utilized in Ref. [77] was identical to the matrix polymer of the present work, and also most experimental conditions were the same.) We just recall that the crosslinking efficiency, i.e., the percentage of DMMI moieties which leads to elastically effective crosslinks upon complete photodimerization, amounts to 16% at 20 g L$^{-1}$, 20% at 40 g L$^{-1}$, 43% at 60 g L$^{-1}$, and 62% at 80 g L$^{-1}$ matrix concentration. Neither the investigations reported in Ref. [77] nor the experiments of the present work showed evidence for syneresis, so that concentrations can be expected to be the same in the sol and the gel state.

Translational diffusion coefficients of the tracer species were measured by FRAP as described in Section 3.2. Experiments were analyzed by the method presented in Ref. [80] particularly with regard to the quantification of distributions of diffusion coefficients. This was necessary since the linear tracers had relatively broad distributions of molecular weights as shown in Table 2.

## 4. Results and discussion

### 4.1. Influence of crosslinking on the diffusion coefficients of linear and spherical tracers

From the FRAP analysis we obtained the distribution of diffusion coefficients [80]. Some typical examples are shown in Fig. 7 in order
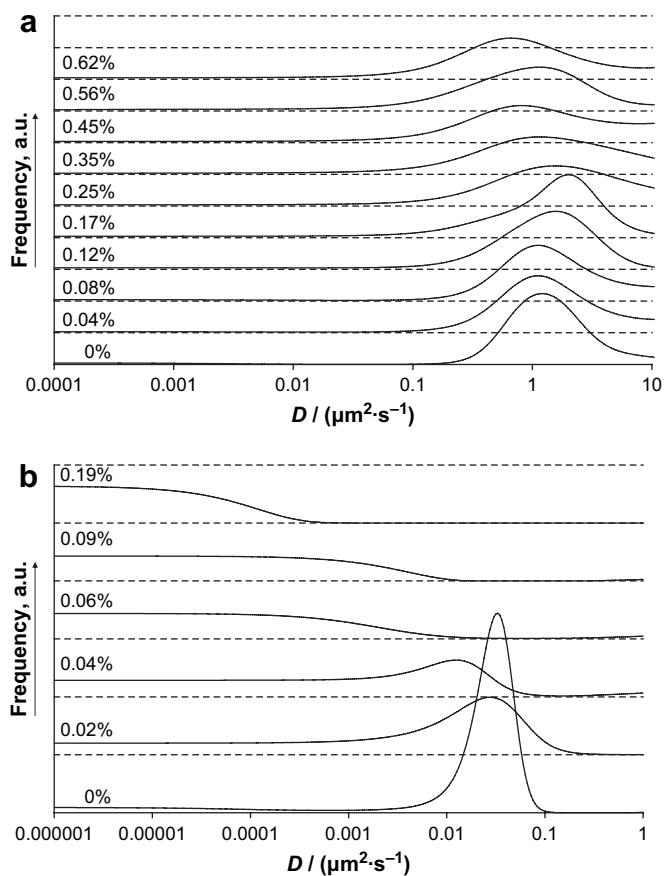


**Fig. 7.** Distributions of the translational diffusion coefficients of (a) 5 g L$^{-1}$ flexible linear PAAm–C0.1–4 ($r_H = 16$ nm) or (b) 0.5 wt.-% rigid spheres ($r_H = 17$ nm) enclosed in 60 g L$^{-1}$ PAAm–DMMI2.0 matrixes at increasing degree of crosslinking, indicated in terms of the number of elastically effective strands (cf. Ref. [77]) divided by the total number of monomer units in percentage quotation. Curves are shifted vertically for greater clarity.

to discuss the characteristic features and the changes that occur when the matrix polymer becomes progressively crosslinked.

When linear tracers were employed (Fig. 7a), we detected a large mobile fraction with diffusion coefficients distributed over the range of $D = 0.1$–$10\ \mu m^2\ s^{-1}$, besides a small portion (1–30%, depending on the particular composition of the sample, typically around 10%) of rather immobile material. (The immobile fraction produces a cusp at the center of the bleached pattern, persisting for long (i.e., infinite) times after complete redistribution of the mobile material.) The portion of the immobile material increased somewhat with rising molar mass of the tracers and rising matrix concentration. However, in no case did it vary systematically with the extent of crosslinking of the matrix. This observation indicates that there was no chemical binding of the tracers to the matrix (due to unwanted side reactions) during photocrosslinking. We assume that the small immobile portion is due to branched rather than linear tracer molecules, which may be formed during the synthesis by chain transfer in free-radical copolymerization (cf. Ref. [78]). Since we are only interested in the behavior of linear tracer molecules, the immobile fraction will be disregarded from now on.

Considering only the mobile fraction, the distribution of the diffusion coefficients of the linear tracers and their mean values exhibit no or just small changes upon crosslinking of the matrix: when matrix concentrations and/or tracer molecular weights are low, there is just some scatter around a mean value and some variation of the width of the distribution, as seen in Fig. 7a. On the other hand, corresponding measurements on samples with higher matrix concentration and/or tracer molecular weights showed a slight decrease of the average diffusion coefficient upon proceeding gelation.

Experiments on samples containing spherical tracers showed a fundamentally different behavior (cf. Fig. 7b): prior to crosslinking, $D$ distributions were solely composed of a well-defined sharp peak in the mobile region, appearing at markedly lower values of $D$ than the corresponding broader ones observed on samples containing linear tracers. Moreover, the dependence of the diffusion coefficient on the concentration of the uncrosslinked matrix was notably stronger for spherical tracers than for linear tracers (see below). With beginning gelation, the amount of mobile spheres is diminished and more and more tracer particles become immobilized, until at a certain threshold of crosslinking there is an abrupt change and all tracers get trapped. As long as mobile tracers could be detected, their mobility seemed to decrease slightly with increasing degree of crosslinking. There was just one exception to this general feature: in the sample consisting of a $20\ g\ L^{-1}$ PAAm matrix (lowest concentration studied), the 17 nm spheres remained equally mobile over the entire crosslinking procedure.

In Fig. 8, the results of various sets of experiments are compared in a systematic way by plotting the mean diffusion coefficients over the degree of crosslinking. The error bars indicate the standard deviations determined when measurements were repeated five times at different, randomly chosen positions (on a mm scale) within one sample at the same crosslinking conversion. Fig. 8a shows the diffusion coefficients for all the different tracers when embedded in a matrix of concentration $40\ g\ L^{-1}$. For the linear tracers having the lower molar masses (uppermost curves), $D$ does not change at all when the matrix is chemically crosslinked, while for the linear tracers with higher molar masses there seems to be a slight but perceptible decrease of $D$ when the crosslinking reaction goes to completion. Concurrently, the spatial variation of $D$ (as indicated by the error bars in Fig. 8) remains small upon matrix-crosslinking for the low molecular weight tracers, whereas $D$ values of the longer tracer chains show perceptible variation when the matrix becomes crosslinked. In any case, however, the molar mass of the tracer molecules has a bigger impact on their diffusion coefficients than the fact that the matrix is crosslinked or not. On
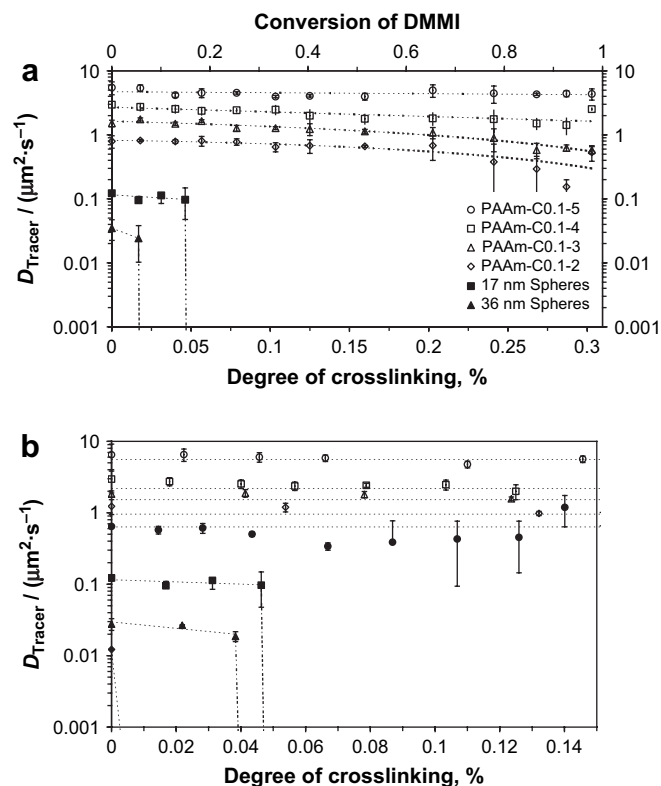


**Fig. 8.** Average values of the translational diffusion coefficients of linear polyacrylamides and spherical polystyrene particles during gradual crosslinking of a surrounding PAAm matrix. (a) System composed of $40\ g\ L^{-1}$ PAAm–DMMI2.0 containing differently sized linear (open symbols) and spherical (full symbols) tracers. (Note that the coils of PAAm–C0.1–4 and PAAm–C0.1–3 have comparable size to the 17 and 36 nm spheres, respectively.) (b) Comparison of linear PAAm–C0.1–4 (open symbols) and 17 nm spheres (full symbols) in surrounding PAAm–DMMI2.0 matrixes with concentrations of 20 (circles), 40 (squares), 60 (triangles), and $80\ g\ L^{-1}$ (diamonds). In both (a) and (b) values of DMMI conversion (upper axis in (a)) were estimated by UV–vis spectroscopy as described in Section 3.4 and then converted into values of crosslink density (lower axes, denoting the number of elastically effective network chains per total number of monomer units). Error bars are a measure of the spatial variation of $D$ on a mm scale across the sample.

the other hand, the spherical tracers (filled symbols) are only mobile up to a certain extent of crosslinking, which is smaller for the larger spheres.

Fig. 8b illustrates the effect of matrix concentration. The mean diffusion coefficients of the 17 nm spheres (filled symbols) and of the linear tracer PAAm–C0.1–4 (open symbols) are shown in matrixes having concentrations of 20, 40, 60, and $80\ g\ L^{-1}$. The linear tracer was chosen such that its hydrodynamic radius matches that of the hard spheres (cf. Tables 2 and 3). For all matrix concentrations, the diffusion coefficient of the linear tracers remains essentially constant upon gelation. A similar behavior was found for the spheres only in the $20\ g\ L^{-1}$ system (nevertheless, there is some increase of the spatial variation of $D$ upon crosslinking of this sample), while at higher matrix concentrations the mobility of the spheres drops to virtually zero at some characteristic degree of crosslinking, which is the lower the higher the matrix concentration.

Investigations by Lodge, Rotstein, and Won have also shown that the mobility of linear tracers remains almost unaffected by crosslinking of the matrix polymer [68,69,71]. Similar results were obtained by De Smedt et al. [52], while other reports state that the diffusivity of linear tracers decreases appreciably upon crosslinking of the surrounding matrix [55, 66], in contrast to the just quoted and our findings. The fact that the mobility of rigid tracers in a polymer solution is markedly smaller than that of flexible linear

chains has been worked out in several systematic studies where star-shaped polymers or fractal objects were used as probes having intermediate behavior [50,57,60,95].

In order to discuss our results, we consider the relevant length scales of the systems studied. In semidilute solutions, the correlation length $\xi$ is a measure of distance up to which a polymer chain is unaffected by other chains. It can be roughly estimated as [11]

$$\xi_{\text{solution}} \approx R_G \left( \frac{c^*}{c} \right)^\gamma \approx 2.05 \cdot r_H \left( \frac{c^*}{c} \right)^\gamma \tag{5}$$

with $R_G$ being the radius of gyration, $r_H$ the hydrodynamic radius, and $\gamma = 0.75$ as well as $R_G \approx 2.05 r_H$ [96] in good solvents. (Generally, aqueous PAAm solutions near room temperature are considered as being in good solvent. $\chi$-Parameters reported lie in the range of 0.44–0.495 [97–99], while the Mark–Houwink–Sakurada exponent is between 0.7 and 0.8 [100–102].) The $\xi$ values calculated with Eq. (5) using the hydrodynamic radius of the matrix chains are listed in the first column of Table 4. Note that they are in good agreement with dynamic correlation lengths measured by dynamic light scattering on a similar system (data not shown). In most cases, they are smaller than the hydrodynamic radii of the linear or spherical tracers.

Another length scale which becomes relevant after crosslinking is the mean distance between crosslinks. This quantity, denoted as $\xi_x$, could be obtained from the molar concentration of elastically effective junctions, which was in turn deduced from modulus measurements [77], according to

$$\xi_x = \sqrt[3]{\frac{1}{c_{\text{junctions}} N_A}} \tag{6}$$

The corresponding data listed in the second column of Table 4 are those for the fully crosslinked gels. The fact that the network density grows in direct proportion with DMMI conversion [77] can be used to determine the mean distance between crosslinks at intermediate stages.

The $\xi_{\text{solution}}$ and $\xi_x$ data are strikingly similar. The difference between the semidilute solution and the fully crosslinked gel is therefore not a change of the characteristic length scale, but solely the fact that the inter-chain interaction is temporary and fluctuating (in solution) or permanent (in a gel). This difference seems to be rather irrelevant for the mobility of the linear tracers, presumably because of their high internal flexibility and dynamics.

The rigid spherical particles, on the other hand, are markedly affected by permanent crosslinks: they get trapped when the crosslink density exceeds a certain threshold. The mean distances between crosslinks at the experimentally observed thresholds were calculated for the two sizes of spheres studied and are also listed in Table 4, Columns 3 and 4. These critical distances between crosslinks seem to be fairly independent of matrix concentration (there is quite some variation), but are correlated with the size of the spheres, as one would expect on grounds of a very simplistic

picture. An exception to this behavior was merely found for the system composed of 20 g L$^{-1}$ PAAm2.0 with 17 nm spheres (cf. Fig. 8b), where the mesh size in the gel state seems to be sufficiently large to allow for diffusion of the spheres.

Konak Bansil, and collaborators also addressed the subject of varying the ratio between the mesh size of a chemical network and the size of rigid or flexible tracers enclosed [67,70,72,103]. Their results are qualitatively similar to ours. Since these networks were made by crosslinking copolymerization, network heterogeneity was large and the degree of crosslinking was not so well defined. To our knowledge, the present work is the first which *quantitatively* relates the critical mesh size for tracer immobilization to the diameter of the probes making use of an independent characterization of network architecture.

## 4.2. Concentration and molecular weight dependence of the diffusion coefficients in semidilute solutions

In Fig. 9, all diffusion coefficients determined in uncrosslinked matrixes are plotted as a function of matrix concentration in order to compare the experimental results with theoretical predictions. Also included are the data in dilute (matrix-free) solution.

Since the main emphasis of our work was on studying the effect of crosslinking, the data obtained on uncrosslinked samples are rather limited and do not allow for an in-depth inspection of concentration or molar mass dependencies. However, we feel that some major features can be discussed with appropriate care.
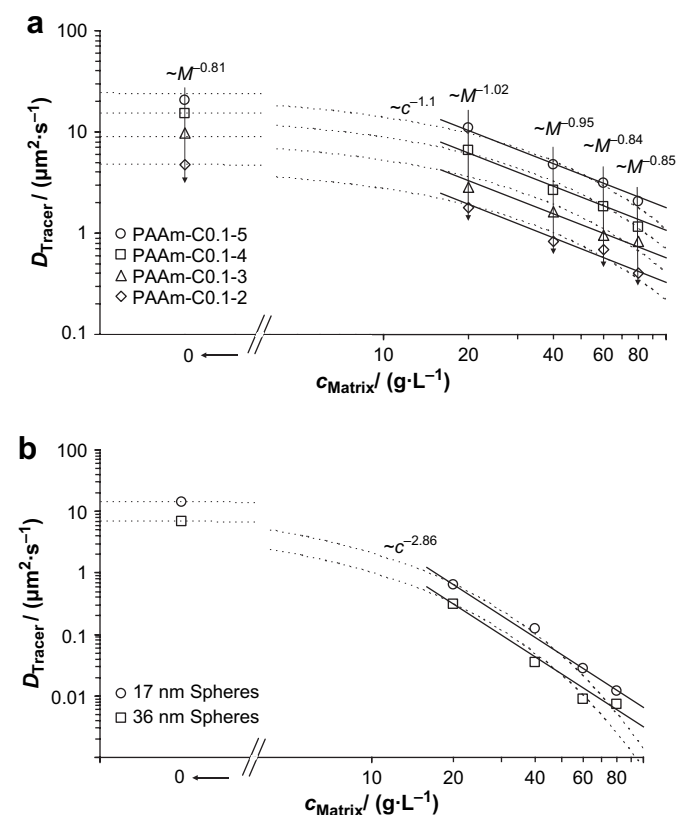
**Table 4**
Average mesh sizes in aqueous semidilute solutions ($\xi_{\text{solution}}$) and chemically crosslinked hydrogels ($\xi_x$) of PAAm–DMMI2.0

| $c_{\text{matrix}}$ (g L$^{-1}$) | $\xi_{\text{solution}}$[a] (nm) | $\xi_x$[b] (nm) | $\xi_{\text{17 nm spheres immobile}}$[b] (nm) | $\xi_{\text{36 nm spheres immobile}}$[b] (nm) |
|---|---|---|---|---|
| 20 | 16.0 | 17.2 | No immobilization | 33.0 |
| 40 | 9.5 | 12.5 | 25.2 | 32.8 |
| 60 | 7.0 | 8.5 | 27.7 | 48.8 |
| 80 | 5.7 | 6.9 | 24.8 | 44.3 |

Also listed are the values at the level of crosslinking where the mobilities of enclosed 17 and 36 nm spheres drop to zero.

[a] Calculated from Eq. (5), utilizing $c^{*c}$ and $r_H$ from Table 2.
[b] Calculated from Eq. (6) on the basis of rheology results as reported in Ref. [77].



**Fig. 9.** Diffusion coefficients of differently sized linear (a) and spherical (b) tracers as a function of the concentration of a surrounding PAAm matrix. In both (a) and (b), $D$ values are the ones prior to matrix-crosslinking. Both plots also contain the values of the pure tracers in the absence of a surrounding matrix. Relations between $D$ and $c$ are analyzed by the application of power laws in the semidilute domain (full lines) as well as Phillies' universal scaling equation in the form of Eq. (3a) over the entire range of matrix concentration (dotted lines) in both cases. Moreover, (a) also contains an indication of the corresponding power law dependences of $D$ on $M_W$ (arrows).

In Fig. 9a, the course of the diffusion coefficients of the linear tracers over matrix concentration is compared with Phillies' formula, Eq. (3a) (dotted lines). For the fit curves, the same values of $\alpha = 0.1$ and $\nu = 0.8$ are presumed. When the four curves were fitted individually, the parameters show a broad scatter, $0.04 \leq \alpha \leq 0.25$ instead of the common value 0.1, and $0.54 \leq \nu \leq 0.97$ instead of the common value 0.8, but no systematic variation with molar mass of the tracers. The combined fit therefore seems to be more appropriate. The fit curves show reasonable agreement with the experimental data, although the curvature in the semidilute regime seems to be too strong.

The full straight lines shown in Fig. 9a represent the scaling behavior in the semidilute regime. They are drawn with a common slope of $-1.10$ as a result of a combined fit, while individual fits had slopes between $-0.94$ and $-1.18$. This is definitely steeper than $-0.5$ as predicted for an unentangled semidilute solution in a good solvent (Eq. (2a)). On the other hand, it is just the predicted value for a $\theta$ solvent, but this solution state is not anticipated for aqueous PAAm solutions. As an alternative, one may argue that the value around $-1$ lies *between* the predicted values for unentangled ($-0.5$) and entangled ($-1.75$) solutions in a good solvent, and that the solutions investigated exhibit a gradual change between the two regimes in the concentration range inspected because of the broad molar mass distribution of the PAAm employed.

Also indicated in Fig. 9a are the exponents obtained when molar mass dependencies were analyzed. In the semidilute regime, they are in the range between $-0.84$ and $-1.02$. This is in close agreement with scaling predictions for the unentangled semidilute state (Eq. (2)). Note, however, that the corresponding exponent found in dilute solution is $-0.81$ instead of the expected $-0.6$. Besides the fact that only very few data points were available, it should be kept in mind that the molar mass distributions of the linear tracers (and also that of the matrix polymer) were relatively broad, and that the weight averages used were determined by SEC employing a pullulan calibration, which may have led to additional errors.

Fig. 9b contains the data for the spherical tracers as well as the corresponding fit curves. The dotted lines were obtained by application of Phillies' approach with $\alpha = 0.4$ and $\nu = 0.7$. Again, they seem to be curved too strongly in the semidilute range. The full lines, on the other hand, assume a power law behavior with an exponent around $-2.86$, indicating a much stronger concentration dependence for the spheres than for the flexible, linear tracers. In terms of Phillies' approach, this fact is captured by the parameter $\alpha$, which changes from 0.1 for the linear tracers to 0.4 for the spheres, while the parameter $\nu$ is hardly affected. Since only two sizes of spheres were studied, the size dependence cannot be considered.

## 5. Conclusions

The investigation of the diffusion of mesoscopic probes in semidilute uncrosslinked and crosslinked polymer systems has revealed the following observations:

1. In semidilute polymer solutions, the diffusion coefficient of hard spheres is markedly smaller than that of flexible linear macromolecules having a similar coil size in terms of radius of gyration.
2. The concentration dependence of the diffusion coefficient in solution is much stronger for spheres than for flexible linear chains.
3. Crosslinking of the semidilute matrix has only a minor influence on the diffusion of linear tracers or no effect at all, while the spherical tracers get completely immobilized when the degree of crosslinking exceeds the particular threshold where the mesh size becomes comparable to the size of the probes.

In view of these observations, one has to conclude that the rate-determining mechanism of diffusion processes is fundamentally different for the two kinds of probes. The mobility of hard spheres is solely controlled by the structure and dynamics of the surrounding matrix, while for linear macromolecules, the internal flexibility and dynamics of the probes have a major, decisive influence. This statement is well accepted for concentrated solutions or polymer melts, where the motions of linear chains occur via the reptation mechanism. Our experiments, however, cover the semidilute regime with polymer concentration being only 4–16 times higher than the overlap concentration, which is commonly assumed just to be the *onset* of entanglement effects. The exponents found for the molar mass dependence of the diffusion coefficient and for its concentration dependence, despite the uncertainty due to broad distributions, also seem to indicate that the systems studied are below the entanglement concentration. Nevertheless, the observation that the diffusion coefficient of linear chains is practically the same in uncrosslinked and crosslinked matrixes, where the hydrodynamic radius of the probe molecules is substantially larger than the mesh size, points to the fact that the translational mobility of the chains is governed by their intramolecular mobility. In order to enable the molecules to move through the permanent meshes, a mechanism somehow similar to reptation needs to be envisaged.

The hydrodynamic scaling model predicts that the translational mobilities of flexible coils and of hard spheres having a comparable size are similar. Our results clearly exclude such behavior in the concentration range studied, although the equation proposed provides a reasonable fit to the individual data sets.

## References

[1] Graessley WW. Adv Polym Sci 1974;16:1.
[2] Tirrell M. Rubber Chem Technol 1984;57:523.
[3] Pearson DS. Rubber Chem Technol 1987;60:439.
[4] Skolnick J, Kolinski A. Adv Chem Phys 1989;78:223.
[5] Lodge TP, Rotstein NA, Prager S. Adv Chem Phys 1990;79:1.
[6] Watanabe H. Prog Polym Sci 1999;24:1253.
[7] McLeish TCB. Adv Phys 2002;51:1379.
[8] Masaro L, Zhu XX. Prog Polym Sci 1999;24:731.
[9] De Gennes PG. J Chem Phys 1971;55:572.
[10] De Gennes PG. Macromolecules 1976;9:587, 594.
[11] De Gennes PG. Scaling concepts in polymer physics. London: Cornell University Press; 1979.
[12] Edwards SF. J Phys A 1975;8:1670.
[13] Doi M, Edwards SF. J Chem Soc Faraday Trans II 1978;74:1789, 1802, 1818.
[14] Doi M, Edwards SF. The theory of polymer dynamics. Oxford: Clarendon Press; 1986.
[15] Brochard F, De Gennes PG. Macromolecules 1977;10:1157.
[16] Schaefer DW, Joanny JF, Pincus P. Macromolecules 1980;13:1280.
[17] Graessley WW. Adv Polym Sci 1982;47:67.
[18] Doi M. J Polym Sci Part B Polym Phys 1983;21:667.
[19] Phillies GDJ, Ullmann GS, Ullmann K, Lin TH. J Chem Phys 1985;82:5242.
[20] Phillies GDJ. Macromolecules 1986;19:2367.
[21] Phillies GDJ. Macromolecules 1987;20:558.
[22] Phillies GDJ. Macromolecules 1988;21:3101.
[23] Phillies GDJ. J Phys Chem 1989;93:5029.
[24] Phillies GDJ. J Phys Chem 1992;96:10061.
[25] Phillies GDJ, Quinlan CA. Macromolecules 1995;28:160.
[26] Phillies GDJ. arXiv:cond-mat/0403109; 2004.
[27] Hervet H, Leger L, Rondelez F. Phys Rev Lett 1979;42:1681.
[28] Leger L, Hervet H, Rondelez F. Macromolecules 1981;14:1732.
[29] Marmonier MF, Leger L. Phys Rev Lett 1985;55:1078.
[30] Amis EJ, Han CC. Polymer 1982;23:1403.

[31] Amis EJ, Han CC, Matsushita Y. Polymer 1984;25:650.
[32] von Meerwall ED, Amis EJ, Ferry JD. Macromolecules 1985;18:260.
[33] Callaghan PT, Pinder DN. Macromolecules 1984;17:431.
[34] Fleischer G, Straube E. Polymer 1985;26:241.
[35] Brown W, Zhou P. Macromolecules 1989;22:4031.
[36] Brown W, Zhou P. Macromolecules 1989;22:3508.
[37] Wesson JA, Noh I, Kitano T, Yu H. Macromolecules 1984;17:782.
[38] Antonietti M, Coutandin J, Gruetter R, Sillescu H. Macromolecules 1984;17:798.
[39] Kim HD, Chang TH, Yohanan JM, Wang LX, Yu H. Macromolecules 1986;19:2737.
[40] Wang FW, Lowry RE. Polymer 1985;26:1654.
[41] Numasawa N, Kuwamoto K, Nose T. Macromolecules 1986;19:2593.
[42] Smith DE, Perkins TT, Chu S. Phys Rev Lett 1995;75:4146.
[43] Gorti S, Ware BRJ. Chem Phys 1985;83:6449.
[44] Phillies GDJ, Malone C, Ullmann K, Ullmann GS, Rollings J, Yu LP. Macromolecules 1987;20:2280.
[45] Phillies GDJ, Pirnat T, Kiss M, Teasdale N, Maclung D, Inglefield H, et al. Macromolecules 1989;22:4068.
[46] Phillies GDJ, Gong J, Li L, Rau A, Zhang K, Yu LP, et al. J Phys Chem 1989;93:6219.
[47] Wattenberger MR, Bloomfield VA, Bu Z, Russo BS. Macromolecules 1992;25:5263.
[48] Onyenemezu CN, Gold D, Roman M, Miller WG. Macromolecules 1993;26:3833.
[49] Oikawa H, Nakanishi H. J Chem Phys 2001;115:3785.
[50] Cheng Y, Prud'homme RK, Thomas JL. Macromolecules 2002;35:8111.
[51] De Smedt SC, Lauwers A, Demeester J, Engelborghs Y, De Mey G, Du M. Macromolecules 1994;27:141.
[52] De Smedt SC, Meyvis TKL, Demeester J, Van Oostveldt P, Blonk JCG, Hennink WE. Macromolecules 1997;30:4863.
[53] Gribbon P, Hardingham TE. Biophys J 1998;75:1032.
[54] Gribbon P, Heng BC, Hardingham TE. Biophys J 1999;77:2210.
[55] Burke MD, Park JO, Srinivasarao M, Khan SA. Macromolecules 2000;33:7500.
[56] Perry PA, Fitzgerald MA, Gilbert RG. Biomacromolecules 2006;7:521.
[57] Lodge TP, Wheeler LM. Macromolecules 1986;19:2983.
[58] Lodge TP, Markland P. Polymer 1987;28:1377.
[59] Wheeler LM, Lodge TP, Hanley B, Tirrell M. Macromolecules 1987;20:1120.
[60] Lodge TP, Markland P, Wheeler LM. Macromolecules 1989;22:3409.
[61] Phillies GDJ. Macromolecules 1990;23:2742.
[62] Phillies GDJ, Brown W, Zhou P. Macromolecules 1992;25:4948.
[63] Wheeler LM, Lodge TP. Macromolecules 1989;22:3399.
[64] Furukawa R, Arauz-Lara JL, Ware BR. Macromolecules 1991;24:599.
[65] Liu R, Gao X, Adams J, Oppermann W. Macromolecules 2005;38:8845.
[66] Antonietti M, Sillescu H. Macromolecules 1985;18:1162.
[67] Bansil R, Pajevic S, Konak C. Macromolecules 1990;23:3380.
[68] Lodge TP, Rotstein NA. J Non-Cryst Solids 1991;131–133:671.
[69] Rotstein NA, Lodge TP. Macromolecules 1992;25:1316.
[70] Pajevic S, Bansil R, Konak C. Macromolecules 1993;26:305.
[71] Won J, Lodge TP. J Polym Sci Part B Polym Phys 1993;31:1897.
[72] Kuo CS, Bansil R, Konak C. Macromolecules 1995;28:768.
[73] Wentzel D, Oppermann W. Colloid Polym Sci 1997;275:205.
[74] Pluen A, Netti PA, Jain RK, Berk DA. Biophys J 1999;77:542.
[75] Fatin-Rouge N, Starchev K, Buffle J. Biophys J 2004;86:2710.
[76] Song Q, Zhang G, Wu C. Macromolecules 2007;40:8061.
[77] Seiffert S, Oppermann W, Saalwächter K. Polymer 2007;48:5599.
[78] Seiffert S, Oppermann W. Macromol Chem Phys 2007;208:1744.
[79] Seiffert S, Oppermann W. J Microsc 2005;220:20.
[80] Hauser GI, Seiffert S, Oppermann W. J Microsc 2008;230:353.
[81] Kronfeld KP, Timpe HJ. J Prakt Chem 1988;330:571.
[82] Wöhrle D, Tausch MW, Stohrer WD. Photochemie. Weinheim: Wiley-VCH; 1998.
[83] Herkstroeter WG, Lamola AA, Hammond GS. J Am Chem Soc 1964;86:4537.
[84] Allonas X, Ley C, Bibaut C, Jacques P, Fouassier JP. Chem Phys Lett 2000;322:483.
[85] Steinmetz R. Fortschr Chem Forsch 1967;7:445.
[86] Lewis FD, Saunders WH. J Am Chem Soc 1968;90:7033.
[87] Krystkowiak E, Maciejewski A, Kubicki J. ChemPhysChem 2006;7:597.
[88] von Sonntag J, Knolle W. J Photochem Photobiol A Chem 2000;136:133.
[89] Soni VK, Stein RS. Macromolecules 1990;23:5257.
[90] Geissler E, Horkay F. Macromolecules 1991;24:543.
[91] Hecht AM, Horkay F, Geissler E. J Phys Chem B 2001;105:5637.
[92] Kizilay MY, Okay O. Macromolecules 2003;36:6856.
[93] Nie J, Du B, Oppermann W. Macromolecules 2004;37:6558.
[94] Liu R, Oppermann W. Macromolecules 2006;39:4159.
[95] Baille WE, Zhu XX, Fomine S. Macromolecules 2004;37:8569.
[96] Burchard W. Adv Polym Sci 1999;143:113.
[97] Silberberg A, Eliassaf J, Katchalksy A. J Polym Sci 1959;23:259.
[98] Misra GS, Bhattacharya SN. Eur Polym J 1979;15:125.
[99] Day JC, Robb ID. Polymer 1981;22:1530.
[100] Scholtan W. Makromol Chem 1954;14:169.
[101] Klein WM, Conrad M. Makromol Chem 1978;179:1635.
[102] McCarthy KJ, Burkhardt CW, Parazak DP. J Appl Polym Sci 1987;33:1699.
[103] Reina JC, Bansil R, Konak C. Polymer 1990;31:1038.